ACS APPLIED MATERIALS & INTERFACES

Research Article

Cite This: ACS Appl. Mater. Interfaces XXXX, XXX, XXX–XXX

www.acsami.org

Tailoring Permeability of Microporous Copper Structures through Template Sintering

Chi Zhang,[†] James W. Palko,[†,‡] Guoguang Rong,[†] Kenneth S. Pringle,[†] Michael T. Barako,[†,∥] Thomas J. Dusseault,[†] Mehdi Asheghi,[†] Juan G. Santiago,[†] and Kenneth E. Goodson*[,†]

[†]Department of Mechanical Engineering, Stanford University, Stanford, California 94305, United States

[‡]Department of Mechanical Engineering, University of California-Merced, Merced, California 95340, United States

[∥]NG Next Basic Research Laboratory, Northrop Grumman Corporation, Redondo Beach, California 90278, United States

Supporting Information

ABSTRACT: Microporous metals are used extensively for applications that combine convective and conductive transport and benefit from low resistance to both modes of transport. Conventional fabrication methods, such as direct sintering of metallic particles, however, often produce structures with limited fluid transport properties due to the lack of control over pore morphologies such as the pore size and porosity. Here, we demonstrate control and improvement of hydraulic permeability of microporous copper structures fabricated using template-assisted electrodeposition. Template sintering is shown to modify the fluid transport network in a manner that increases permeability by nearly an order of magnitude with a less significant decrease (~38%) in thermal conductivity. The measured permeabilities range from 4.8×10^{-14} to 1.3×10^{-12} m^2 with 5 μm pores, with the peak value being roughly 5 times larger than the published values for sintered copper particles of comparable feature sizes. Analysis indicates that the enhancement of permeability is limited by constrictions, i.e., bottlenecks between connecting pores, whose dimensions are highly sensitive to the sintering conditions. We further show contrasting trends in permeability versus conductivity of the electrodeposited microporous copper and conventional sintered copper particles and suggest these differing trends to be the result of their inverse structural relationship.

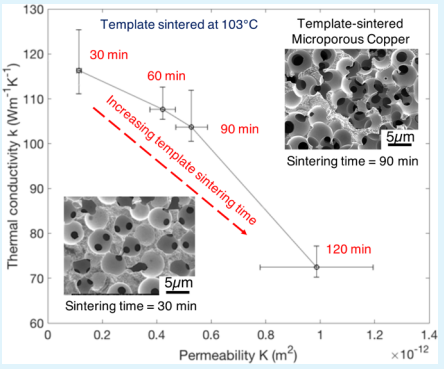

KEYWORDS: *microporous copper, permeability, conductivity, porosity, sintering*

INTRODUCTION

Microporous metals are utilized in a large range of applications, including active and passive heat exchange technologies,[1−7] battery electrodes,[8,9] electrochemical sensors,[10,11] and liquid and vapor phase catalysis.[12,13] The need to simultaneously transport fluid through the pore space and energy or charge through the matrix to a surface where they interact is a common requirement across these applications. Microporous metals feature high specific surface area,[14] high thermal[15,16] and electrical[8,15] conductivity, and good interconnectivity of pores.[17] This desirable combination of properties, thus, makes them well suited for use as porous wicking structures in two-phase thermal management systems such as heat pipes[18] and vapor chambers[19] due to their potential to minimize the transport resistances associated with heat conduction, liquid delivery, and vapor removal. The porous wicks serve the dual purpose of transporting working fluid through capillary-driven flow, while simultaneously supplying heat flow to extended phase-change surfaces. The maximum capillary-limited heat flux sustained by heat pipes and vapor chambers is reached when the viscous pressure drop in the wick structure exceeds the available capillary pressure generated by the porous wick.[20] The thermal conductance of the wick itself plays an important role in facilitating heat spreading and maximizing the thermally accessible area of the phase-change interface. Therefore, when designing high-performance passive electronic cooling devices, wick structures that combine the advantages of high capillary pressure, high permeability, and low thermal resistance are of particular interest.

A number of previous studies reported sintered screen meshes,[21,22] open-cell metal foams,[23,24] and linear grooves and channels[25] as wick structures for capillary-driven heat exchangers. However, the limited capillary performances of these materials have restricted the maximum sustainable heat fluxes to less than 200 W cm^{-2} and resulted in gravitational-dependent operation. As small feature sizes are desired to increase the capillarity of the wick, many studies have used sintered copper powders[26−28] (particle diameter ranging from tens of microns to submillimeter) as wicks to improve capillary-limited heat flux up to ~600 W cm^{-2}. Sintering of metal powders, however, typically requires high temperatures (550−950 °C) and tightly controlled ambient conditions.[20]

Received: March 6, 2018
Accepted: August 10, 2018
Published: August 10, 2018

DOI: 10.1021/acsami.8b03774
ACS Appl. Mater. Interfaces XXXX, XXX, XXX–XXX

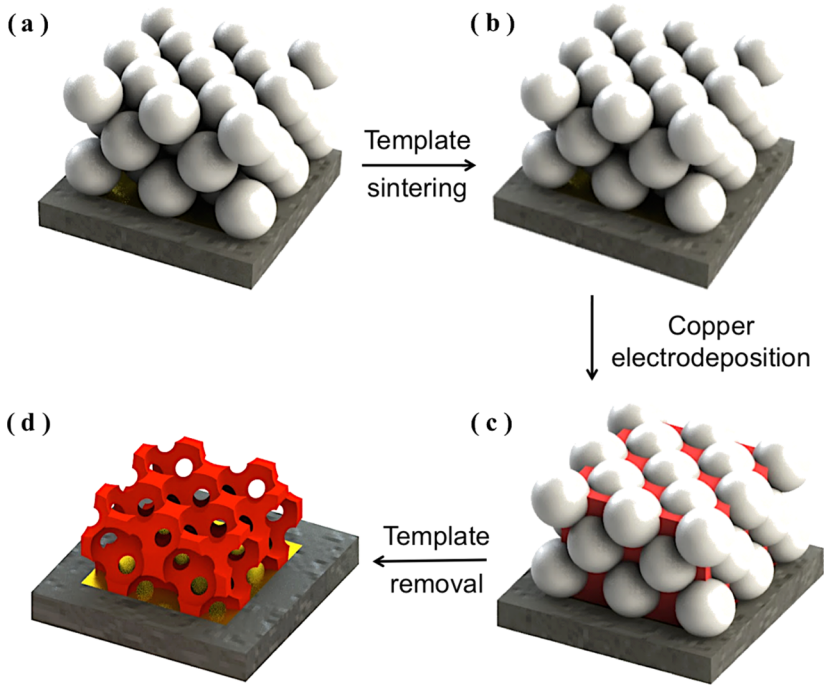

Figure 1. Schematic illustration of the method used to prepare electrodeposited microporous copper with template sintering modulations. (a) Self-assembly of colloidal spheres of 5 μm averaged diameter that creates point contacts with adjacent particles. (b) Bonded areas (not shown) between neighboring spheres are enlarged during template sintering due to particle coalescence, accompanied by macroscopic template densification. (c) Electrodeposition of copper in the interstitials of the sintered template. (d) Selective dissolution of the polystyrene template in an organic solvent bath results in fluid-permeable microporous structures.

Due to the large distribution of copper particle sizes, nonspherical particle shapes, and the semiconsolidated nature of the sintered beds, precise control over pore morphologies and ultra-thin wick form factors (e.g., <100 μm thick) proves to be challenging.[20,29,30] For a fixed particle size range, the permeability of sintered copper powders does not show a clear trend with sintering conditions, which is indicative of random variability in particle size and shape.[20]

Metal electrodeposition around a sacrificial template offers an alternative approach to the fabrication of high capillary pressure wick structures at low temperatures (<110 °C), while simultaneously allowing for elaborate control over pore morphology and wick thickness of the final microstructure.[8,9,15,31] Template-assisted microporous structures are prepared by assembling colloidal spheres, depositing metals in the gaps, and then selectively removing the template leaving structures with spherical pores.[32] Due to precise tunability of template self-assembly,[16,17,33−35] pore sizes ranging from tens of nanometers to a few microns are readily controlled,[34,36] which brings benefits of high surface area and high capillarity to two-phase heat exchange applications.

To improve the fluid transport properties of microporous structures, we incorporate template sintering as a strategy to modulate the size of circular "necks" that bridge the adjacent spherical pores of the microstructure, as shown in Figure 1. During template heating, polystyrene spheres with a 5 μm averaged diameter merge with neighboring particles accompanied by a gradual increase in their contacting areas. The coalescence of the two adjacent spherical particles at elevated temperatures driven by surface diffusion, grain boundary diffusion, and/or a combination of both mechanisms have been discussed extensively in previous studies.[37−40] This diffusion controlled process results in an overall template densification and an associated decrease in the void volume at elevated temperatures.[39,41] The decreased void volume in the template then translates to an increased void volume fraction (i.e., porosity) and interconnected nature of inverse structures.

Previous investigations have demonstrated the feasibility of tailoring the hydraulic permeability of microporous copper structures by applying annealing processes to the initial polymer template.[42] However, there is a need for a theoretical model that directly links the template fabrication parameters to the permeability of microporous copper structures. To better design materials that target the specific and often competing thermofluidic properties required in complex heat transfer systems, a more complete understanding of the fluid and thermal characteristics of template-sintered microporous copper structures is essential. In this work, we present both modeling and experimental results to reveal the effect of template sintering on the thermophysical properties of microporous copper structures. Permeability is measured using a flow geometry through the in-plane direction of the thin films with a focus on the impact of template sintering parameters. We analyze the changes in neck (i.e., contacting area between the adjacent pores) diameters of the microporous copper structures via scanning electron microscopy (SEM) and attribute the enhancement in permeability to an increase in neck sizes directly resulting from initial template sintering. Furthermore, we measure the electrical conductivity of the microporous structures tuned by template sintering and examine the correlation of changes in permeability and thermal conductivity with template modification. We show this correlation to differ markedly from that observed in traditional, directly sintered copper powders, and provide an explanation for this difference based on the underlying inverse microstructures of these two material classes.

DOI: 10.1021/acsami.8b03774
ACS Appl. Mater. Interfaces XXXX, XXX, XXX−XXX

EXPERIMENTAL METHOD

We prepare working electrodes for copper electrodeposition by sputtering a titanium adhesion layer (10 nm) followed by a gold seed layer (50 nm) on 2 cm × 2 cm square silicon substrates. Polystyrene spheres with an averaged diameter of 5 μm are synthesized via dispersion polymerization,[43] and self-assemble into random-packed structures using drop-casting.[17,42]

We sinter the assembled polymer templates at temperatures of 95, 103, and 110 °C (±0.5 °C) in a furnace (Fisher Scientific Isotemp), which is maintained at the targeted sintering temperature for various periods of time (referred to as "sintering time"). Over the entire heating process, the temperature of sintering is monitored closely by two T-type thermocouples attached to the sample substrates. After the sintering process, a small drop of ethanol (5 μL) is wicked into the sintered template before immersing it in an aqueous electrolyte solution (0.6 M $CuSO_4$ + 5 mM H_2SO_4) for copper electrodeposition. We utilize a three-electrode poly(tetrafluoroethylene) electrolytic setup[16] with a 1.2 cm × 1.2 cm electrodeposition area in the center of silicon substrates. Copper is electrodeposited to infiltrate the sintered template using potentiostatic deposition for 40 min,[42] which yields microporous copper structures with a thickness of 20 ± 1 μm.

Permeability Measurements. We measure the in-plane permeability of microporous copper structures using a plastic manifold pressed onto the microporous copper films (see, Supporting Information S1 and S2).[44] Steady pressure drops of air flow imposed by the manifold traversing the porous film are measured at various flow rates, and linear regression of pressure drop to flow rate determines the permeability (as shown in Figure S4). In the Darcy regime where inertial and compressibility effects are negligible, permeability K of a porous structure is defined as

$$K = f\mu \frac{Q}{A} \frac{L}{(P_{in} - P_{out})} \tag{1}$$

here, Q (m^3 s^{-1}) is the volumetric flow rate supplied to the microporous structure, μ (Pa·s) is air viscosity, A (m^2) is the cross-sectional area of the flow pathway within the porous medium, L (m) is the distance between which the pressure drop occurs, and f is a scaling factor that accounts for flow fringing compared to a nominal one-dimensional flow geometry (see Supporting Information S2). Pressure drops for the imposed flow rates are less than 15 kPa, resulting in negligible compressibility effects. The maximum Reynolds number for the flows measured (based on the nominal 5 μm pore size) is less than 0.03, which also verifies the laminar flow regime. Inertial effects are negligible for gas flows in porous media in this regime.[45]

Porosity Measurements. The polystyrene template sintering at elevated temperatures is accompanied by template densification (i.e., a decrease void volume in template) with increasing sintering time, which later translates to an increased void volume fraction (i.e., porosity) and interconnected nature of the inverse structure. It is thus of interest to characterize the dependence of porosity on sintering parameters. The porosity of the microporous copper structure is calculated using a differential mass method as

$$\varepsilon = \frac{V_V}{V_T} = 1 - \frac{m_{Cu}/\rho_{Cu}}{A_s d_s} \tag{2}$$

here, V_T is the bulk or total volume of the microporous copper film and V_V is the volume of void-space in the porous medium. The mass of copper, m_{Cu}, is the differential mass of the sample substrate prior and after copper electrodeposition. The area of the microporous copper structure, A_s, and the thickness, d_s, are obtained using a profilometer (Bruker Dektak 150).

Conductivity Measurements. Electrical conductivity of the microporous copper structures is measured using a standard four-point probe method. Serpentine paths are patterned with laser cutting (Figure S5) to improve measurement sensitivity from the same samples sintered at 103 °C. With a width of ∼1 mm and a total length of ∼2.5 cm, each sample has a resistance on the order of ∼0.1 Ω. Since the copper layer is over 300 times thicker than the titanium/gold seed layer, conductance contribution of the seed layer proves to be negligible. By measuring the exact geometric dimensions of the serpentine pattern, we can directly calculate the electrical conductivity σ as

$$\sigma = \frac{L_s}{R_s w_s d_s} \tag{3}$$

here, R_s is the measured resistance of the serpentine pattern sample, L_s and w_s are the total length and width of the serpentine conductive path, whereas d_s is the thickness of the copper thin film. Electrical conductivity is averaged over at least six measurements for each sample.

We further derive thermal conductivity (k) from electrical conductivity (σ) using the Wiedemann–Franz law,[46] which denotes the ratio of the electronic contribution of the thermal conductivity of a metal to its electrical conductivity is proportional to temperature

$$\frac{k}{\sigma} = LT \tag{4}$$

The Wiedemann–Franz law correlating thermal and electrical conductance of metal microstructures with characteristic dimensions higher than ∼200 nm is satisfied at room temperatures.[47] Experimental Lorenz number L of copper is given as 2.23 × 10^{-8} W Ω K^{-2}.[46] Direct thermal and electrical characterization of copper inverse opal structures using a similar copper electrodeposition method has shown good consistency with the Wiedemann–Franz law.[15]

RESULTS AND DISCUSSION

Figure 2 shows the plot of measured permeability as a function of template sintering time for different sintering temperatures.

The microporous copper structure without template sintering modification presents an enormous hydraulic resistance ($K \sim 10^{-14}$ m^2) due to highly disconnected internal pores. In contrast, the microporous copper structures with template sintering modifications show significant improvement in measured permeability by almost 2 orders of magnitude,

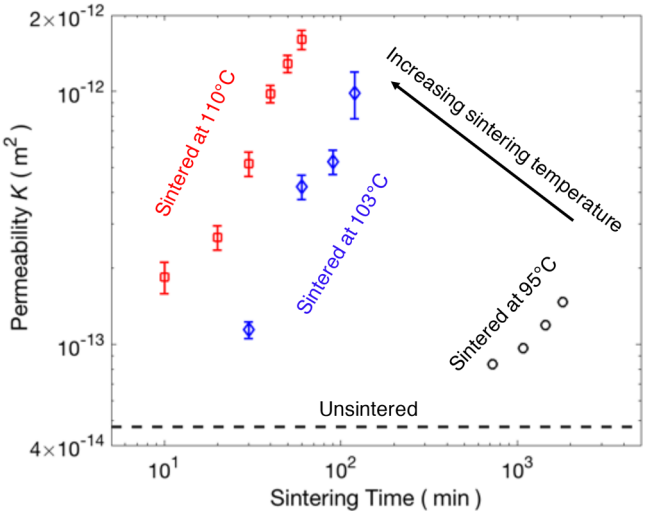

Figure 2. Permeability versus template sintering time for microporous copper structures at sintering temperatures of 95 °C (black markers), 103 °C (blue markers), and 110 °C (red markers). Uncertainties in permeability values are evaluated based on 90% confidence intervals for the linear fit of pressure drop to flow rate. Uncertainties for samples with template sintered at 95 °C are smaller than the symbol size.

DOI: 10.1021/acsami.8b03774
ACS Appl. Mater. Interfaces XXXX, XXX, XXX−XXX

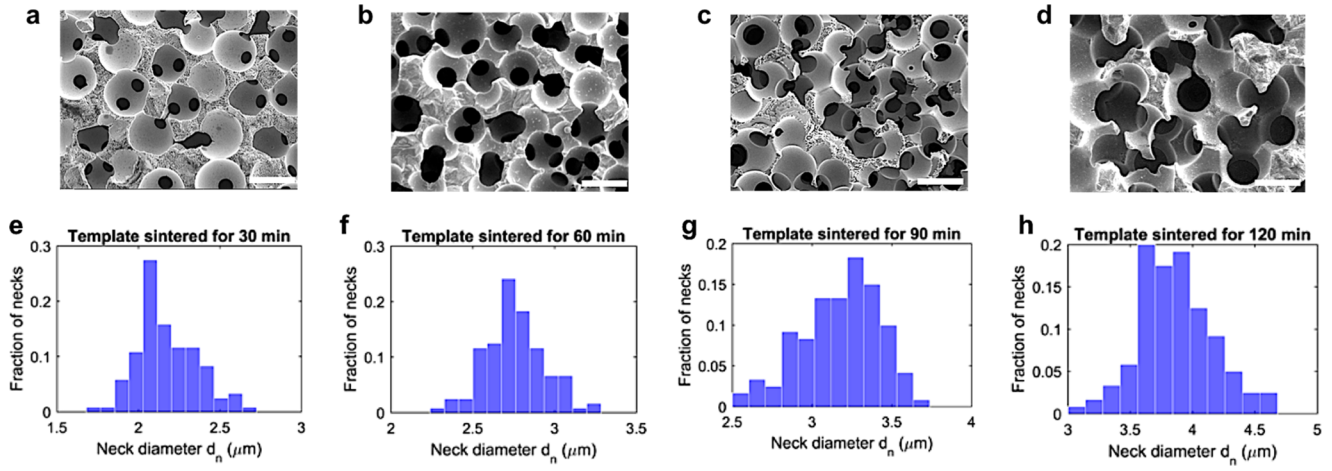

Figure 3. Enhancement of porous copper permeability via template sintering is analyzed by identifying the enlargement of circular necks that connect spherical pores with one another in the copper microstructures. (a–d) Representative SEM images of microporous copper samples with the template sintered at 103 °C for 30, 60, 90, and 120 min, respectively. The growth of interconnected necks (dark circles) bridging the adjacent pores allows fluid to permeate through the porous matrix. (e–h) Histograms of neck diameter distribution of the corresponding porous copper samples (a–d) are obtained by statistically sampling more than 200 neck diameters from SEM images taken at more than 10 random locations of each samples. All scale bars are 5 μm.

owning to the consistent growth of neck diameters with sintering time. In particular, template sintering at temperatures higher than the glass transition temperature of polystyrene (T_g ~ 100 °C) markedly promotes efficiency for permeability modulation by decreasing annealing time from days to tens of minutes. This is mainly due to the reduction of polystyrene viscosity above T_g that facilitates sphere coalescence.[41] It should also be noted that upper limits of template sintering conditions (time and temperature) exist to maintain desirable structural continuity of the microporous copper films, as gas evolution and pore closure of templates are usually encountered at aggressive sintering temperatures or for extensively long periods.[39,41]

We analyze the enhancement of porous copper permeability via template sintering by identifying the enlargement of circular necks that connect spherical pores with one another in this microstructure. As flow resistance scales inversely with the square of the fluid path diameter, "bottlenecks" along the flow would dominate the total flow rate. It is thus reasonable to analyze the permeability of our porous copper structure by characterizing the narrowest constrictions encountered by the flow, which are the necks between connecting pores. This bottleneck assumption has been utilized by Despois and Mortensen[48] for the permeability of open-cell microcellular materials, which showed good agreement with the experimental data for low-density metal foams. Although bottleneck diameters in these metal foams were not directly quantified due to the random nature and nonspherical shape of the necks,[48] for our porous copper structure with spherical pores, we can carefully examine the circular necks owning to our fine control over the microstructure facilitated by the template-assisted fabrication method. We statistically measure neck diameters (number of necks sampled >200) from SEM images taken at more than 10 random locations of each samples, and generate the distribution of neck diameter as shown in Figure 3 and Table 1. Assuming that the necks dominate the flow resistance, we directly correlate permeability with a microscopic neck diameter d_n as (see Supporting Information S6 for detailed derivation)

Table 1. Characteristics of Template-Sintered Microporous Copper Samples Shown in Figure 3

Figure 3	sintering condition	permeability K (m^2)	averaged neck diameter d_n (μm)	standard deviation of d_n (μm)
a	103 ± 0.5 °C 30 min	1.15×10^{-13}	2.17	0.17
b	103 ± 0.5 °C 60 min	4.21×10^{-13}	2.76	0.18
c	103 ± 0.5 °C 90 min	5.27×10^{-13}	3.17	0.24
d	103 ± 0.5 °C 120 min	9.86×10^{-13}	3.86	0.30

$$K = \frac{d_n^3 \varepsilon}{4\pi d_p} \quad (5)$$

where ε is the porosity of the porous copper structure, d_p is the averaged pore diameter.

Figure S8 features the porosity measurement results of microporous copper structures with the template sintered at 103 °C. As expected, the longer the sintering time, the denser the sacrificial polystyrene template, the higher the porosity of a porous copper sample. We compare the experimental permeability data for microporous copper samples with template sintered at 103 °C with predictions using the bottleneck model in eq 5, shown in Figure 4. This model underpredicts permeability values when using the mean neck diameters, with the difference being less than 45% of the experimentally measured values for the four samples plotted. We note that the distribution of neck diameters accounts primarily for this discrepancy, as necks with diameters larger than average would significantly reduce the flow resistance ($\Delta P \sim 1/d_n^3$), leading to a higher measured permeability value. Furthermore, if such larger necks were to randomly connect with one another, then in the microporous structure percolating fluid pathways are formed, which act as flow "shortcuts" and can effectively enhance the permeability. This is especially true for samples that have undergone more aggressive template sintering, as evidenced by structural

DOI: 10.1021/acsami.8b03774
ACS Appl. Mater. Interfaces XXXX, XXX, XXX–XXX

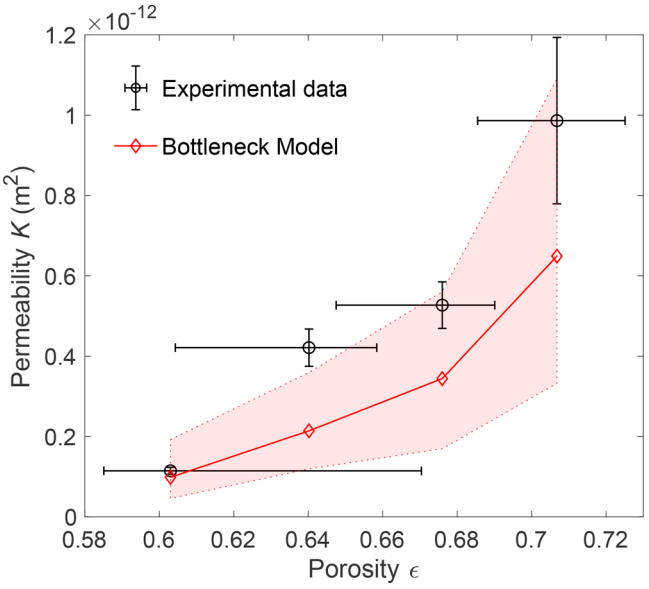

Figure 4. Permeability of microporous copper scaling with porosity for samples with template sintering temperature of 103 °C. As the sintering time of opal template increases, the permeability of the resulting inverse structures improves accompanied by an increase in porosity. The bottleneck model (using the averaged neck diameter values) underpredicts permeability values, with the difference being less than 45% of the experimentally measured values. The bottleneck model computed using the maximum and minimum neck diameters analyzed for each sample is plotted in the filled red band, which indicates the upper and lower limit of the predicted permeabilities.

discontinuity observed using SEM (such as Figure 3d). To account for the nonuniform neck diameter distribution, the maximum and minimum d_n from the statistical analysis are used to estimate the upper and lower limit of permeability values, respectively, as indicated in the filled red band in Figure 4. The computed range demonstrates the strong dependence of permeability on pore morphologies such as the neck diameter and porosity of the microporous structures.

Thermal conductivity values for samples with template sintered at 103 °C are shown in Figure S9, and results are plotted as a function of porosity. In general, the thermal conductivity decreases as the sintering time increases, opposite to the permeability trends. The sample sintered at 103 °C for 120 min shows a 37.7% reduction for thermal conductivity compared to the sample sintered for 30 min (also at 103 °C), while the permeability increases by ~9 times (shown in Figure 2). Direct thermal conductivity measurements using a 3ω method on porous copper of a higher (i.e., 0.74) and a lower (i.e., 0.53) porosity have been performed,[15,16] with thermal conductivities measured to be 62 and 170 W m^{-1} K^{-1}, respectively. The results of thermal conductivity calculations in the present work lie within the range of these thermal measurements.

Effective medium theory is widely used to model the composite properties of porous media, where the geometric arrangement and the composition of the components are commonly considered. In the case of porous copper, due to the tortuosity of the three-dimensional conduction pathway, the length of the conduction pathway is subsequently increased.[15] This macroscopic bending of current leads to further reduction in conductivity in addition to solid volume fraction scaling, as described by Maxwell for conduction in a binary porous medium with a uniform arrangement of spherical pores[49,50]

$$\sigma_{\text{eff,Maxwell}} = \sigma_{\text{Cu}}\left(\frac{2\Phi}{3-\Phi}\right) = \sigma_{\text{Cu}}\left(\frac{2-2\varepsilon}{2+\varepsilon}\right) \quad (6)$$

The experimental data in this work show agreement with the Maxwell's model to be within 15%, as shown in Figure S9.

On the basis of dimensional analysis, the permeability of a porous medium is proportional to the square of its characteristic dimension, typically taken as the averaged particle or pore size.[51] This has been demonstrated numerically for both the sintered particle wicks and inverse wicks.[45] To compare porous structures of vastly different feature sizes, we normalize permeability using the particle/pore diameter such that the normalized permeability ($K^* = K/d^2$) is only dependent on the porosity of the structures. Figure 5 shows a correlation of the

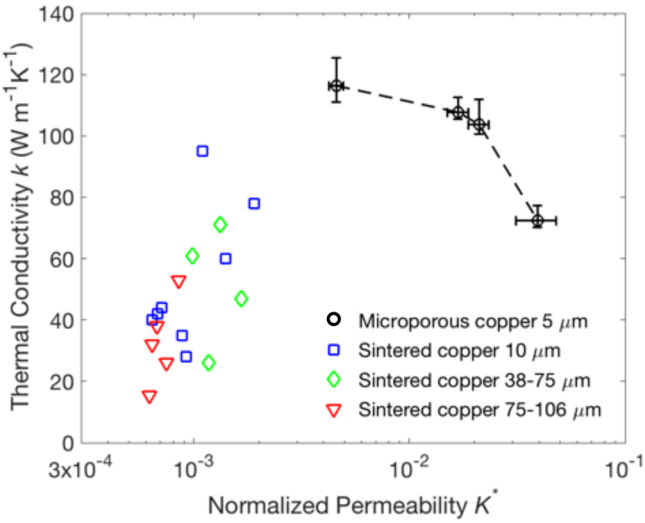

Figure 5. Thermal conductivity and normalized permeability of template-sintered microporous copper in comparison with sintered copper powder.[20] Normalized permeability is given by $K^* = K/d^2$, where d is the averaged particle or pore diameter. The pore diameter of the microporous copper in this work is 5 μm, while particle diameters for sintered copper wicks are 10, 38−75, and 75−106 μm, respectively.

derived thermal conductivity versus normalized permeability for the porous copper structures formed with templates sintered for varying times. For a fixed pore size of 5 μm, template modification allows variation of permeability over approximately an order of magnitude with relatively modest changes in thermal conductivity (from 116 to 72 W m^{-1} K^{-1}). For comparison, Figure 5 also shows the thermal conductivity versus normalized permeability reported in the literature for a number of different porous copper structures formed by direct sintering of copper particles,[20] which are widely employed as porous wicks in thermal management devices. These sintered copper structures of different particle sizes all show a far stronger negative correlation between thermal conductivity and permeability at a fixed particle diameter range. Sintering of copper powders can effectively increase the thermal conductivity from 15 to 92 W m^{-1} K^{-1}, but normalized permeability only varies within a small range (less than a factor of 3) for a given particle size. This difference between electrodeposited microporous copper and sintered copper can be understood based on the structural modifications that occur

DOI: 10.1021/acsami.8b03774
ACS Appl. Mater. Interfaces XXXX, XXX, XXX−XXX

during the sintering of the template particles used to define the microporous copper compared to the copper particles, which directly comprise the sintered copper structures.

As the sacrificial template is sintered, the bonded area between the adjacent spheres increases. This translates to wider necks bridging neighboring pores in the resulting electrodeposited copper, reducing the area along the flow paths that are obstructed by the thin membrane defining the neck, but less strongly affecting the solid filaments of the structure along which conduction occurs (Figure 1d). In contrast, the directly sintered particle compacts result in the inverse structure relying on particle−particle contact for conduction. Sintering in these structures will increase the particle contact area, with a concomitant increase in thermal conductivity but relatively small changes in permeability, which is controlled by the interstices between the particles.

The scaling of normalized permeability with porosity of porous media is dependent on structural morphologies. In Figure 6, we compare our results for template-sintered porous

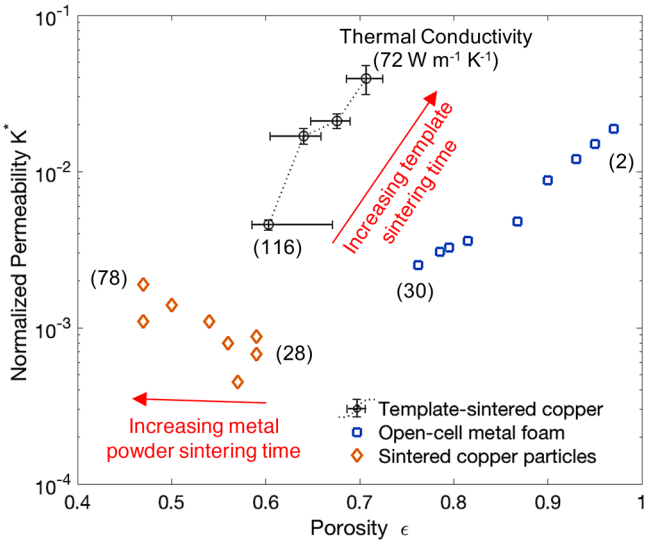

Figure 6. Normalized permeability with respect to porosity for template-sintered microporous copper in comparison with sintered copper powders and metal foams. Normalized permeability is given by $K^* = K/d^2$, where d is the averaged particle or pore diameter. The averaged pore diameter of template-sintered microporous copper is 5 μm, whereas the averaged particle diameter for sintered copper wicks is 10 μm.[20] Metal foams have an averaged pore diameter of 400 μm.[48] Variations of the thermal conductivities of template-sintered microporous copper, sintered copper powders,[20] and metal foams[52,53] scaling with porosity are included for comparison.

copper structures with permeability measurements reported for sintered copper particles and metal foams. As the sintering temperature or time increases, the copper particles under direct sintering become more closely arranged, which in turn decreases the porosity. This effect, however, is reversed for template-sintered microporous wicks, which show an increasing porosity with the sintering time. The normalized permeability of sintered copper particles under different sintering conditions stochastically vary within a small range, suggesting that improving the hydraulic transport capability of sintered copper structures predominantly rely on increasing the averaged copper particle size, as plotted in Figure S10. Template-sintered microporous copper, however, offers tunable permeability in a broad range (e.g., K^* ranging from 0.004 to 0.04) at a given pore size with template sintering modifications. In addition, the attainable permeability of microporous copper with template sintering is shown to be substantially greater than that of sintered particle wicks of similar feature sizes. Such improvement in normalized permeability is comparable to that of metal foams, which also feature an open-pore configuration albeit with much larger pore diameters (typically hundreds of microns to a few millimeters). High porosities of metal foams, however, result in less superior thermal conductivities. As small feature sizes of porous media provide advantageous capillary pressure and specific surface area, template-sintered microporous copper structures featuring micron-level pore sizes, high hydraulic permeability and thermal conductivity are extremely appealing for two-phase thermal management systems.

SUMMARY AND CONCLUSIONS

We report the capability of tailoring the hydraulic permeability of microporous copper structures by optimizing the template sintering process. This template modification allows more than an order of magnitude increase in permeability associated with the widening of necks between the adjacent pores of the structure. Using this approach, permeabilities are observed to be an order of magnitude larger than those for directly sintered powder-based porous metals with similar feature sizes. The increase in permeability for porous copper with template modification is accompanied by a much smaller decrease in conductivity (e.g., ~40%). This behavior is in sharp contrast to that of traditional powder-based porous metals, which show a strong increase in conductivity with sintering but a small decrease in permeability. We attribute these trends to the approximately inverse relationship between the geometries of these materials.

The ability to tune permeability with the minimal effect on conductivity provides a useful design parameter for electronic cooling systems using porous metals, and is complementary to the minimal control offered by powder-based materials for fixed feature sizes. The fabrication method also offers significant advantages in terms of low temperature processing (~100 °C) and the ability to produce thin films (e.g., <20 μm). These capabilities enable enhanced performance in a number of applications such as thermofluidic heat exchangers and two-phase electronic cooling.

ASSOCIATED CONTENT

Supporting Information

The Supporting Information is available free of charge on the ACS Publications website at DOI: 10.1021/acsami.8b03774.

Permeability measurement setup, Darcy flow simulation of actual flow geometry, linear relationship of pressure drop versus flow rate, serpentine pattern for electrical conductivity characterization, image analysis of neck diameters, derivation of permeability using the "bottle-neck model", porosity measurement results, conductivity measurement results, feature size square dependence of permeability for sintered copper particles (PDF)

AUTHOR INFORMATION

Corresponding Author

*E-mail: goodson@stanford.edu.

DOI: 10.1021/acsami.8b03774
ACS Appl. Mater. Interfaces XXXX, XXX, XXX−XXX

ORCID

Chi Zhang: 0000-0001-8711-1974
Michael T. Barako: 0000-0002-4745-4515

Notes

The authors declare no competing financial interest.

■ ACKNOWLEDGMENTS

This work was partially funded by the Defense Advanced Research Projects Agency under award number HR0011-13-2-0011. C.Z. is thankful for the financial support from the Stanford School of Engineering Graduate Fellowship. G.R. would like to acknowledge support from the Shanghai International Science and Technology Collaboration Program under Grant 13430710400. K.S.P. acknowledges support from the National Science Foundation Engineering Research Center for Power Optimization of Electro Thermal Systems (POETS) with cooperative agreement EEC-1449548. Part of this work was performed at the Stanford Nano Shared Facilities (SNSF), supported by the National Science Foundation under Award no. ECCS-1542152.

■ REFERENCES

(1) Kim, J.; You, S.; Choi, S. U. Evaporative Spray Cooling of Plain and Microporous Coated Surfaces. *Int. J. Heat Mass Transfer* **2004**, *47*, 3307−3315.
(2) El-Genk, M. S.; Ali, A. F. Enhanced Nucleate Boiling on Copper Micro-Porous Surfaces. *Int. J. Multiphase Flow* **2010**, *36*, 780−792.
(3) Khodabandeh, R.; Furberg, R. Heat Transfer, Flow Regime and Instability of a Nano-and Micro-Porous Structure Evaporator in a Two-Phase Thermosyphon Loop. *Int. J. Therm. Sci.* **2010**, *49*, 1183−1192.
(4) Rainey, K.; You, S. Pool Boiling Heat Transfer from Plain and Microporous, Square Pin-Finned Surfaces in Saturated Fc-72. *J. Heat Transfer* **2000**, *122*, 509−516.
(5) Xu, J.; Ji, X.; Zhang, W.; Liu, G. Pool Boiling Heat Transfer of Ultra-Light Copper Foam with Open Cells. *Int. J. Multiphase Flow* **2008**, *34*, 1008−1022.
(6) Oh, J.; Zhang, R.; Shetty, P. P.; Krogstad, J. A.; Braun, P. V.; Miljkovic, N. Thin Film Condensation on Nanostructured Surfaces. *Adv. Funct. Mater.* **2018**, *28*, No. 1707000.
(7) Palko, J.; Zhang, C.; Wilbur, J.; Dusseault, T.; Asheghi, M.; Goodson, K.; Santiago, J. Approaching the Limits of Two-Phase Boiling Heat Transfer: High Heat Flux and Low Superheat. *Appl. Phys. Lett.* **2015**, *107*, No. 253903.
(8) Zhang, H.; Yu, X.; Braun, P. V. Three-Dimensional Bicontinuous Ultrafast-Charge and-Discharge Bulk Battery Electrodes. *Nat. Nanotechnol.* **2011**, *6*, 277−281.
(9) Armstrong, E.; McNulty, D.; Geaney, H.; O'Dwyer, C. Electrodeposited Structurally Stable V2o5 Inverse Opal Networks as High Performance Thin Film Lithium Batteries. *ACS Appl. Mater. Interfaces* **2015**, *7*, 27006−27015.
(10) Lee, Y. J.; Braun, P. V. Tunable Inverse Opal Hydrogel Ph Sensors. *Adv. Mater.* **2003**, *15*, 563−566.
(11) Tiemann, M. Porous Metal Oxides as Gas Sensors. *Chem. -Eur. J.* **2007**, *13*, 8376−8388.
(12) Umeda, G. A.; Chueh, W. C.; Noailles, L.; Haile, S. M.; Dunn, B. S. Inverse Opal Ceria−Zirconia: Architectural Engineering for Heterogeneous Catalysis. *Energy Environ. Sci.* **2008**, *1*, 484−486.
(13) Zou, R. Q.; Sakurai, H.; Xu, Q. Preparation, Adsorption Properties, and Catalytic Activity of 3d Porous Metal-Organic Frameworks Composed of Cubic Building Blocks and Alkali-Metal Ions. *Angew. Chem.* **2006**, *118*, 2604−2608.
(14) Banhart, J. Manufacture, Characterisation and Application of Cellular Metals and Metal Foams. *Prog. Mater. Sci.* **2001**, *46*, 559−632.
(15) Barako, M. T.; Sood, A.; Zhang, C.; Wang, J.; Kodama, T.; Asheghi, M.; Zheng, X.; Braun, P. V.; Goodson, K. E. Quasi-Ballistic Electronic Thermal Conduction in Metal Inverse Opals. *Nano Lett.* **2016**, *16*, 2754−2761.
(16) Barako, M. T.; Weisse, J. M.; Roy, S.; Kodama, T.; Dusseault, T. J.; Motoyama, M.; Asheghi, M.; Prinz, F. B.; Zheng, X.; Goodson, K. E. In *Thermal Conduction in Nanoporous Copper Inverse Opal Films*, IEEE Intersociety Conference on Thermal and Thermomechanical Phenomena in Electronic Systems; IEEE, 2014; pp 736−743.
(17) Dusseault, T. J.; Gires, J.; Barako, M. T.; Won, Y.; Agonafer, D. D.; Asheghi, M.; Santiago, J. G.; Goodson, K. E. In *Inverse Opals for Fluid Delivery in Electronics Cooling Systems*, IEEE Intersociety Conference on Thermal and Thermomechanical Phenomena in Electronic Systems; IEEE, 2014; pp 750−755.
(18) Sobhan, C.; Rag, R.; Peterson, G. A Review and Comparative Study of the Investigations on Micro Heat Pipes. *Int. J. Energy Res.* **2007**, *31*, 664−688.
(19) Weibel, J. A.; Garimella, S. V. Recent Advances in Vapor Chamber Transport Characterization for High-Heat-Flux Applications. In *Advances in Heat Transfer*; Elsevier, 2013; pp 209−301.
(20) Espinosa, F. A. D.; Peters, T. B.; Brisson, J. G. Effect of Fabrication Parameters on the Thermophysical Properties of Sintered Wicks for Heat Pipe Applications. *Int. J. Heat Mass Transfer* **2012**, *55*, 7471−7486.
(21) Li, C.; Peterson, G.; Wang, Y. Evaporation/Boiling in Thin Capillary Wicks (L)—Wick Thickness Effects. *J. Heat Transfer* **2006**, *128*, 1312−1319.
(22) Li, C.; Peterson, G. Evaporation/Boiling in Thin Capillary Wicks (Ii)—Effects of Volumetric Porosity and Mesh Size. *J. Heat Transfer* **2006**, *128*, 1320−1328.
(23) Han, X.-H.; Wang, Q.; Park, Y.-G.; T'Joen, C.; Sommers, A.; Jacobi, A. A Review of Metal Foam and Metal Matrix Composites for Heat Exchangers and Heat Sinks. *Heat Transfer Eng.* **2012**, *33*, 991−1009.
(24) Lu, W.; Zhao, C.; Tassou, S. Thermal Analysis on Metal-Foam Filled Heat Exchangers. Part I: Metal-Foam Filled Pipes. *Int. J. Heat Mass Transfer* **2006**, *49*, 2751−2761.
(25) Launay, S.; Sartre, V.; Lallemand, M. Experimental Study on Silicon Micro-Heat Pipe Arrays. *Appl. Therm. Eng.* **2004**, *24*, 233−243.
(26) Weibel, J. A.; Garimella, S. V.; North, M. T. Characterization of Evaporation and Boiling from Sintered Powder Wicks Fed by Capillary Action. *Int. J. Heat Mass Transfer* **2010**, *53*, 4204−4215.
(27) Semenic, T.; Lin, Y. Y.; Catton, I.; Sarraf, D. B. Use of Biporous Wicks to Remove High Heat Fluxes. *Appl. Therm. Eng.* **2008**, *28*, 278−283.
(28) Weibel, J. A.; Kousalya, A. S.; Fisher, T. S.; Garimella, S. V. In *Characterization and Nanostructured Enhancement of Boiling Incipience in Capillary-Fed, Ultra-Thin Sintered Powder Wicks*, IEEE Intersociety Conference on Thermal and Thermomechanical Phenomena in Electronic Systems; IEEE, 2012; pp 119−129.
(29) Bodla, K. K.; Weibel, J. A.; Garimella, S. V. Advances in Fluid and Thermal Transport Property Analysis and Design of Sintered Porous Wick Microstructures. *J. Heat Transfer* **2013**, *135*, No. 061202.
(30) Bodla, K. K.; Murthy, J. Y.; Garimella, S. V. Direct Simulation of Thermal Transport through Sintered Wick Microstructures. *J. Heat Transfer* **2012**, *134*, No. 012602.
(31) Pham, Q.; Barako, M.; Tice, J.; Won, Y. Microscale Liquid Transport in Polycrystalline Inverse Opals across Grain Boundaries. *Sci. Rep.* **2017**, *7*, No. 10465.
(32) Waterhouse, G. I.; Waterland, M. R. Opal and Inverse Opal Photonic Crystals: Fabrication and Characterization. *Polyhedron* **2007**, *26*, 356−368.
(33) Mandlmeier, B.; Szeifert, J. M.; Fattakhova-Rohlfing, D.; Amenitsch, H.; Bein, T. Formation of Interpenetrating Hierarchical Titania Structures by Confined Synthesis in Inverse Opal. *J. Am. Chem. Soc.* **2011**, *133*, 17274−17282.

DOI: 10.1021/acsami.8b03774
ACS Appl. Mater. Interfaces XXXX, XXX, XXX−XXX

(34) Kim, J.-H.; Kang, S. H.; Zhu, K.; Kim, J. Y.; Neale, N. R.; Frank, A. J. Ni−Nio Core−Shell Inverse Opal Electrodes for Supercapacitors. *Chem. Commun.* **2011**, *47*, 5214−5216.
(35) Kwak, E. S.; Lee, W.; Park, N. G.; Kim, J.; Lee, H. Compact Inverse-Opal Electrode Using Non-Aggregated TiO2 Nanoparticles for Dye-Sensitized Solar Cells. *Adv. Funct. Mater.* **2009**, *19*, 1093−1099.
(36) Graugnard, E.; King, J.; Jain, S.; Summers, C.; Zhang-Williams, Y.; Khoo, I. Electric-Field Tuning of the Bragg Peak in Large-Pore Ti O2 Inverse Shell Opals. *Phys. Rev. B* **2005**, *72*, No. 233105.
(37) Swinkels, F.; Ashby, M. A Second Report on Sintering Diagrams. *Acta Metall.* **1981**, *29*, 259−281.
(38) Zhang, W.; Gladwell, I. Sintering of Two Particles by Surface and Grain Boundary Diffusion−a Three-Dimensional Model and a Numerical Study. *Comput. Mater. Sci.* **1998**, *12*, 84−104.
(39) Greco, A.; Maffezzoli, A. Polymer Melting and Polymer Powder Sintering by Thermal Analysis. *J. Therm. Anal. Calorim.* **2003**, *72*, 1167−1174.
(40) Exner, H. E. Principles of Single-Phase Sintering. *Rev. Powder Metall. Phys. Ceram.* **1979**, *1*, 7−251.
(41) Jayaraman, G. S.; Wallace, J.; Geil, P.; Baer, E. Cold Compaction Molding and Sintering of Polystyrene. *Polym. Eng. Sci.* **1976**, *16*, 529−536.
(42) Zhang, C.; Rong, G.; Palko, J. W.; Dusseault, T. J.; Asheghi, M.; Santiago, J. G.; Goodson, K. E. In *Tailoring of Permeability in Copper Inverse Opal for Electronic Cooling Applications*, ASME 2015 International Technical Conference and Exhibition on Packaging and Integration of Electronic and Photonic Microsystems collocated with the ASME 2015 13th International Conference on Nanochannels, Microchannels, and Minichannels; American Society of Mechanical Engineers, 2015; p V002T06A004.
(43) Song, J. S.; Winnik, M. A. Cross-Linked, Monodisperse, Micron-Sized Polystyrene Particles by Two-Stage Dispersion Polymerization. *Macromolecules* **2005**, *38*, 8300−8307.
(44) Rong, G.; Palko, J. W.; Oyarzun, D. I.; Zhang, C.; Hammerle, J.; Asheghi, M.; Goodson, K. E.; Santiago, J. G. A Method for Quantifying in Plane Permeability of Porous Thin Films. *J. Colloid Interface Sci.* **2018**, *530*, 667−674.
(45) Ngo, I.-L.; Byon, C. Permeability of Microporous Wicks with Geometric Inverse to Sintered Particles. *Int. J. Heat Mass Transfer* **2016**, *92*, 298−302.
(46) Kittel, C. *Introduction to Solid State Physics*; Wiley, 2005.
(47) Stojanovic, N.; Maithripala, D.; Berg, J.; Holtz, M. Thermal Conductivity in Metallic Nanostructures at High Temperature: Electrons, Phonons, and the Wiedemann-Franz Law. *Phys. Rev. B* **2010**, *82*, No. 075418.
(48) Despois, J.-F.; Mortensen, A. Permeability of Open-Pore Microcellular Materials. *Acta Mater.* **2005**, *53*, 1381−1388.
(49) Maxwell, J. C. *A Treatise on Electricity and Magnetism*; Clarendon, 1892; Vol. *1*.
(50) Aichlmayr, H. T.; Kulacki, F. The Effective Thermal Conductivity of Saturated Porous Media. *Adv. Heat Transfer* **2006**, *39*, 377−460.
(51) Dullien, F. A. *Porous Media: Fluid Transport and Pore Structure*; Academic Press, 2012.
(52) Yang, X.; Kuang, J.; Lu, T.; Han, F.; Kim, T. A Simplistic Analytical Unit Cell Based Model for the Effective Thermal Conductivity of High Porosity Open-Cell Metal Foams. *J. Phys. D: Appl. Phys.* **2013**, *46*, No. 255302.
(53) Paek, J.; Kang, B.; Kim, S.; Hyun, J. Effective Thermal Conductivity and Permeability of Aluminum Foam Materials. *Int. J. Thermophys.* **2000**, *21*, 453−464.

DOI: 10.1021/acsami.8b03774
ACS Appl. Mater. Interfaces XXXX, XXX, XXX−XXX